Flow Regimes and Storage Efficiency of CO_2 Injected into Depleted Shale Reservoirs

Evgeniy M. Myshakin,[a,b*] Harpreet Singh,[a,c] Sean Sanguinito,[a,b] Grant Bromhal,[a] Angela L. Goodman[a]

[a] U.S. Department of Energy, National Energy Technology Laboratory, 626 Cochrans Mill Road, Pittsburgh, PA 15236/3610 Collins Ferry Road, Morgantown, WV 26507

[b]AECOM, 626 Cochrans Mill Road, P.O. Box 10940, Pittsburgh, PA 15236

[c]Oak Ridge Institute for Science and Education, 100 ORAU Way, Oak Ridge, TN 37830, USA

Abstract

Depleted shale reservoirs are potentially attractive targets to store carbon dioxide (CO_2) as free and adsorbed phases. The time-dependent efficiency factors that depict dynamic storage performance in shale are estimated as a function of key reservoir parameters, shapes of stimulated reservoir volume, and injection scenarios. Efficiency of CO_2 storage and flow regimes are determined dynamically as CO_2 is injected in a depleted shale formation for a time period of 60 years. The most effective reservoir utilization for carbon storage was achieved during the transition from predominant flow in the stimulated reservoir volume to flow into unfractured zones. That transition occurs within first 15-30 years of injection depending on cases considered. The importance of adsorption as a mechanism of storage is determined based on sensitivity, which indicates that the amount of CO_2 stored by adsorption would be on average ~26% of the CO_2 stored as a free phase.

Keywords: carbon sequestration; flow regimes; shale; rate transient analysis.

* Corresponding author. Tel.: 1-412-386-5741; fax: 1-412-386-5870.
E-mail address: evgeniy.myshakin@netl.doe.gov

I. Introduction

Commercial production of hydrocarbons from shale formations began just over a decade ago with the advancement of technologies that made producing hydrocarbons from these reservoirs economical. Hydrocarbon production from shale formations in North America, especially in the U.S., demonstrates a sharp rise since then due to drilling of hundreds of thousands of new wells in several shale basins across the U.S. The rate of production from these reservoirs falls very rapidly (generally by more than half within first year [1] compared to conventional reservoirs due to fast depletion of hydrocarbons through fractures. This results in a relatively shorter production life (~5 years) [2] that can be extended to a maximum of ~20 years through enhanced recovery methods [1]. Availability of depleted shale reservoirs presents a promising opportunity for storing CO_2 because of their extremely tight pore space that can act as both a storage reservoir and a seal, with an added benefit of a large number of wells that can be easily converted into CO_2 injectors. Although the research literature on carbon storage in shale is not as exhaustive as its storage in saline aquifers, a few studies have investigated different aspects of storage in shale; sealing integrity of the caprock [3], dynamic response and practicality of large amounts of CO_2 injection in shale gas wells [4], storage capacity in shale [5], and contribution of organic content to storage [6,7]. The outcome of all these studies suggests a possibility of large-scale CO_2 storage in depleted shale gas formations. However, the transport processes by which CO_2 would be stored in depleted shale stratum and their contribution to storage remain poorly understood. This issue has been investigated either for simultaneous production of methane by CO_2 injection [5,8] or through sorption isotherms alone, but it is likely that sorption isotherms alone may not accurately reflect the storage estimates in shale [9]. Schettler and Parmely [5] estimated from sorption isotherms of Devonian shales that contribution of gas storage by open porosity is about 50% and the remaining 50% of storage is intimately associated with adsorption on minerals and organic matter, although this amount could vary with depth and from well to well that presumably change mineralogy or the structure of the shale. Our recent study on this topic [10] investigated time-dependent estimates of efficiency factors for prospective CO_2 storage in depleted shale as free phase and adsorbed phase by accounting for variable properties of shale stratum. Efficiency factors were estimated based on the assumption that CO_2 injected in fractured shales is expected to be stored by sorption on organic matter and clay minerals [9] in addition to its free phase in permeable pores and fractures.

The objective of this study is to investigate the time-dependent efficiency factors that depict dynamic storage performance in shale [10] with the help of rate transient analysis (RTA). Specifically, RTA is used to determine flow regimes and effective permeabilities of fractured shale during injection, which are used to interpret changes in efficiency factors over the injection period of 60 years. Unlike conventional reservoirs, permeability estimates for shale with hydraulically fractured horizontal wells is not straightforward and is affected by induced and natural fracture characteristics, besides other parameters [11-13]. RTA is widely used in the oil and gas industry to predict permeability of a reservoir [14-20], where the unique advantage of the method lies in the fact that it incorporates the in-situ conditions of the formation such as initial pressure, flowing pressure, formation compressibility, etc. However, the original RTA in shale [20] was based on a linear-flow theory that assumes constant compressibility, which is largely valid for liquids, but not for gases or supercritical fluids like carbon dioxide. Further, fractured shale formations are affected in their performance by several variables that include reservoir properties, horizontal well completion, fracture geometry, etc. Therefore, correct representation of RTA in shale requires accounting for non-linear fluid flow, and other parameters related to reservoir and well completion. The RTA method used here accounts for non-linearity in fluid flow through a correction factor term, whereas the effect of reservoir and well completion parameters on RTA is studied exclusively through sensitivity analysis.

II. Volumetric storage equation and associated efficiency terms

A volumetric method incorporating petrophysical parameters and efficiency factors to screen shale formations for prospective CO_2 storage was recently described in three studies [21-23]. The general equation to estimate mass of CO_2 stored in shales is given as follows:

$$G_{CO_2} = V_e\left[\rho_{CO_2}\phi E_\phi + \rho_{sCO_2}(1-\phi)E_S\right] \quad (1)$$

$$V_e = A_t E_A h_g E_h \quad (2)$$

where, G_{CO2} is the CO_2 storage resource (mass) of the shale formation; V_e is the net effective volume of the formation; A_t is the total area (map view) of the shale formation being assessed for CO_2 storage; h_g is the gross thickness of the shale formation; E_A is the fraction of shale formation total area available for CO_2 storage; E_h is the fraction of shale formation gross thickness available for CO_2 storage; ρ_{CO2} is the density of CO_2 at the (averaged) pressure ($\bar{P}$) and (averaged) temperature ($\bar{T}$) of V_e prior to production; ϕ is porosity; ρ_{sCO_2} is the maximum mass of CO_2 sorbed per unit

volume of solid rock, e.g., the asymptotic value of a sorption isotherm; E_ϕ is the fraction of the maximum volume of CO_2 stored as a free phase; and E_S is the fraction of the maximum volume of CO_2 stored as a sorbed phase.

The basic principles and definitions used in the above referenced volumetric method, including for storage in shale [10], are based on Society of Petroleum Engineers (SPE) Storage Resources Management System (SRMS), which is a unified classification system for CO_2 storage estimates [24]. In our previous work [10], we used numerical simulations of CO_2 injection into a depleted shale reservoir to estimate efficiency factors, E_ϕ and E_s, for the above method. The definition of dynamic efficiency factor for storage in pore space of shale is consistent with its definition in saline formations [25,26], while the definition of efficiency factor for storage as an adsorbed phase follows an analogous approach that is given as follows:

$$E_\phi = \frac{V_i^{free}}{V_{max}^{free}} \tag{3}$$

$$E_S = \frac{V_i^{sorb}}{V_{max}^{sorb}} \tag{4}$$

where V_i^{free} and V_i^{sorb} are the simulated CO_2 volumes stored in a reservoir volume contacted by the propagating CO_2 plume as a free gas and a sorbed phase, respectively; V_{max}^{free} and V_{max}^{sorb} are the maximum CO_2 volumes that can be stored in the reservoir volume contacted by the CO_2 plume as a free phase and sorbed phase, respectively, at initial (avearged) $\bar{P}$ and $\bar{T}$ conditions before gas production.

The simulated storage efficiency factors are intended for dry gas shales characterized predominantly by one phase flow in pore space and fractures. CO_2 injection was simulated over a period of 60 years using selected time points, 5, 10, 20, 30, 40, 50, and 60 years to estimate efficiency factors. As a formal requirement, CO_2 injection should be commercially and technically viable on the time scale of site operation. At present, it is difficult to use a common approach to evaluate a time frame required for CO_2 injection into shale reservoirs due large uncertainties in relevant parameters.

The ranges of reservoir's matrix porosity and permeability, density of natural fractures, Langmuir volumes for sorption isotherms, shale thinkness, initial reservoir pressure, injection pressure of CO_2, and shapes of stimulated reservoir volume (SRV) were considered to estimate the effieciency factors. These parameters are considered to be the most important in controlling the fluid transport in shale reservoirs [21, 27]. The values for these parameters were taken as measured or evaluated

quantities for the shale plays [10]. The NFFLOW code [28] used to conduct the simulations considers gas residing in the matrix as a free phase in pore space and fractures, and as a sorbed phase in rock matrix. Sorption is represented by the Langmuir isotherms, where a gas component behaves as a monolayer on a surface. The total amount of gas in each matrix block is considered to be the mass sum of free and sorbed gas. For convinience, the select parameters and the calculated efficeincy factors are given in Tables S1 (Supplemental Materials), respectively.

III. RTA methodology

RTA is broadly used to gauge well performance (and stimulated reservoir volume) by analyzing plots of pseudo rate (normalized by pressure) or pseudo pressure (normalized) *vs* square root of time [14-20]. The application of RTA allows identifying a specific flow regime prevailing at a particular injection time period. To investigate the well and SRV productivity, the method of Wattenbarger et al. [20] serves as an important diagnostic tool that provided the concept of transient flow in shale gas wells by the analysis of (pseudo) pressure-normalized rate versus the square root of time. The corresponding equation for linear flow at constant pressure condition is adapted here for the injection scenario with no skin effect (contribution of formation damage caused by the infiltration of drilling fluids into the pressure drawdown) as follows:

$$x_f \sqrt{k} = f_{cp} \frac{1262 \cdot T}{h\sqrt{(\phi \cdot \mu \cdot c_t)_{wf}}} \frac{1}{m_{cp}} \tag{5}$$

where, x_f is the hydraulic fracture half-length, [ft]; k is the reservoir permeability, [md]; T is the reservoir temperature, [^{o}R]; h is the net-pay reservoir thickness, [ft]; ϕ is the matrix porosity; μ is the injected carbon dioxide viscosity at flowing bottomhole pressure, [cP]; c_t is the total compressibility at initial conditions, [psia^{-1}]; m_{cp} is the slope of the fitted straight line obtained by plotting $\frac{m(P_{wf})-m(P_i)}{q}$ *vs* $\sqrt{t}$, where $m(P_{wf})$ is the real gas pseudo-pressure at flowing bottomhole pressure, [psia^2/cP]; $m(P_{wf})$ is the real gas pseudo-pressure at initial pressure, [psia^2/cP]; q is the gas injection rate, [Mscf/d]; t is time. The real gas pseudo-pressure, $m(P)$, is calculated as:

$$m(P) = 2 \cdot \int_0^P \frac{P}{Z(p) \cdot \mu(p)} dp \tag{6}$$

where $Z(p)$ – pressure-dependent non-ideality correction factor; $\mu(p)$ is the pressure-dependent gas viscosity, [cP], P is pore pressure. The main purpose of pseudo-variables like $m(P)$ is to account for the pressure-dependent variability in gas properties (Z-factor, viscosity, and compressibility) in order to adapt the analytical solutions developed for liquid flow to compressible gas-flow with single-phase [18]. The pseudo-pressure accounts for variation in Z-factor and viscosity of gas, while the changes in gas compressibility are accounted through introduction of pseudo-time, $\sqrt{t_a}$ [29,30]. To address changes in compressibility with pressure, Nobakht and Clarkson [19] reported a correction ($f_{cp} = \sqrt{\frac{(\mu \cdot c_t)_i}{\bar{\mu} \cdot \bar{c_t}}}$) to square-root of time in order to improve the values of $x_f \sqrt{k}$ calculated using the slope (m_{cp}) of the $1/q$ *vs* $\sqrt{t}$ curve. Here, $\bar{\mu}$ and $\bar{c_t}$ are averaged gas viscosity and total compressibility in the region of influence [30]. Ibrahim and Wattenbarger [31,32] also introduced an empirical correction factor (f_{cp}) for a constant flowing pressure conditions:

$$f_{cp} = 1 - 0.0825\, D_D - 0.0857\, D_D^2 \tag{7}$$

where, D_D is the drawdown parameter, which is related to pseudo-pressure at the flowing pressure ($m(P_{wf})$) and initial pressure ($m(P_i)$):

$$D_D = \frac{m(P_{wf}) - m(P_i)}{m(P_{wf})} \tag{8}$$

Both correction factors provide similar behavior over a range of the drawdown parameter under assumption of constant viscosity and gas compressibility dominating total compressibility [19]. In this study, we adopted the correction proposed by Ibrahim and Wattenbarger [31,32] because of its simplicity that does not require estimation of averaged properties to calculate corrected pseudo-time [19]. Equation 5 is a modified form of the original equation that was used for liquid, which is based on linear-flow theory [20]. The original equation for liquid is based on the assumption of constant compressibility of liquid, which is not valid for gases, so the original equation was corrected to account for changing gas compressibility. Although at the bottomhole CO_2 injection occurs at supercritical conditions where carbon dioxide behaves as gas in terms of its viscosity and as liquid in terms of density [33]. Equation 5 is applicable to supercritical CO_2 because the value of the correction factor (f_{cp}) is adjusted accordingly per the properties of CO_2 that are accounted by the pseudo pressure term, which is a function of a compressibility factor term (Z) and viscosity.

166 The pseudo pressure will appropriately account for the properties of CO_2 irrespective of its state
167 that is expected to result in a reasonably accurate correction factor.

168 Flow regimes in unconventional reservoirs are affected by coupled effects of reservoir
169 properties, horizontal well completion, fracture geometry, etc. However, for simplicity and
170 illustrative purposes, we represent transient flow sequence only as a function of pressure
171 distributions within the reservoir model during injection. In case of a vertical well, the completion
172 parameter given by the product $x_f\sqrt{k}$ can be extracted from the linear flow analysis. For a multi-
173 fractured horizontal well, the fracture-half length, x_f, is modified to account for total fracture half-
174 length, *i.e.*, the summation of lengths of all hydraulic fractures $n \cdot x_f$ [18,19], where n is the number
175 of induced fractures spaced far enough to establish a linear transient flow regime within SRV. The
176 graphical representation of this flow regime perpendicular to hydraulic fractures is shown in Fig.
177 1a. The hydraulic fractures create highly permeable pathways for injected fluid that enters SRV
178 around the wellbore. Investigation of simulation results for the cases considered in this study shows
179 that such a flow regime dominates during early years of carbon dioxide injection. It shows that
180 clusters of fractures within a stage can be approximated as one combined conduit acting to inject
181 CO_2 into a stimulated volume between stages. The flow within SRV is defined here as Regime I.
182 As a result, the number of induced fractures (n) estimated from $n \cdot x_f\sqrt{k}$ is considered to be the
183 number of stages.

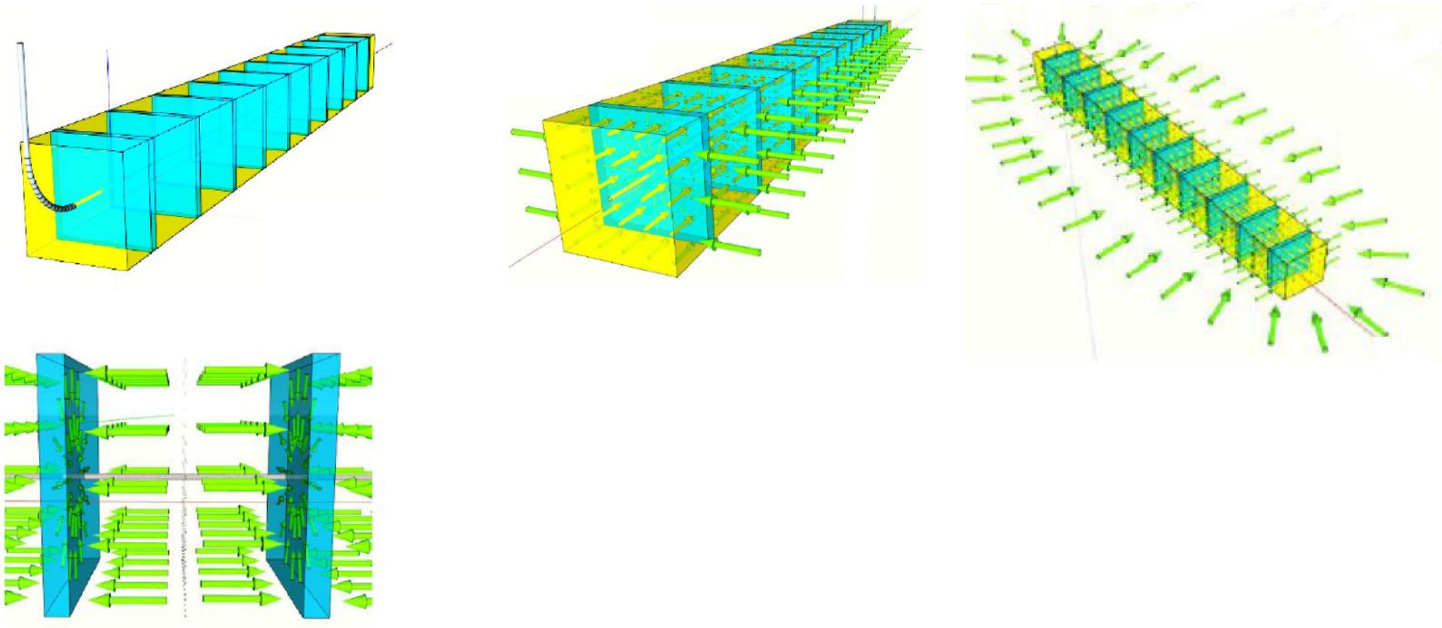

a) Regime I **b) Regime II** **c) Regime III**

Fig. 1. Simplified representation of flow regimes within a shale reservoir: **a)** transverse hydraulic fractures (cyan) forming a rectangular SRV around a lateral (upper) and linear flow inside SRV towards hydraulic fractures (lower); **b)** linear flow inside non-stimulated zone towards SRV; **c)** pseudo-steady radial flow affected by reservoir boundaries inside untreated zone towards SRV (modified from Bahrami et. al. [34]). In case of injection the direction of flow is the opposite.

After pressure buildup within SRV becomes sufficiently high, the next dominant linear flow regime is established towards the reservoir volumes characterized with natural fractures and pore space of rock matrix to transmit fluids outside of SRV (Fig. 1b). In order to estimate effective (bulk) permeability k, the $n \cdot x_f h\sqrt{k}$ product in Equation 5 has to be replaced with the cross-sectional area at well face [17] equal to $2 \cdot x_w h\sqrt{k}$, where x_w is the distance between the center of the first stage and the last stage (762 m (2500 ft)). Next, the pseudo-steady radial flow shown in Fig. 1c (Regime III) was observed at the late injection times and only for a limited number of cases with low matrix porosity and low adsorption. For flow regime that experiences the presence of the reservoir boundaries, $n \cdot x_f h$ is replaced by a reservoir drainage area, A_m [ft^2], (1372 x 1372 m (4500 x 4500 ft)) to calculate k [17,18]. It should be noticed that there are no clearly defined boundaries between Regimes I and II, and II and III, instead the transitions to Regimes II and to III occur over a few years.

IV. Results and Discussion

Bachu et al. [35] indicated that CO_2 storage capacity has a time dependency over the lifetime of a CO_2 storage project and efficiency factors change both temporally and spatially. For saline formations, Gorecki et al. [36] reported storage coefficients at the end of CO_2 injection and as estimated between selected time points "dynamically through injection". Table 1 lists the efficiency factors at discrete times to account for dynamic nature of CO_2 storage per various flow regimes in hydraulically fractured shale. In the beginning of injeciton, induced fractures and natural fracture network act as the main conduit for CO_2 flow. Then, flow through matrix pore volume characterized with permeability on the order of nano-darcy is expected to pick up. Because of diminished permeability, the pressure slowly propagates through the matrix to the outer parts of the reservoir, resulting in transient flow that lasts for a long period of time within a shale reservoir as if it is infinite in size. Later, flow is expected to reach the reservoir's boundaries and

proceeds at pseudo-steady state [17]. Thus, over time CO_2 flows through highly heterogeneous media where a dominant conduit can be induced or natural fractures, with diffusion in matrix pores.

Table 1
Ranges of E_ϕ and E_S efficiency factors for CO_2 storage in shales (Adapted from [10]).

	E_ϕ			
Years	**Minimum**	**Maximum**	**P_{10}***	**P_{90}****
5	0.17	0.56	0.25	0.53
10	0.22	0.59	0.31	0.57
20	0.27	0.60	0.34	0.59
30	0.28	0.60	0.36	0.58
40	0.28	0.59	0.37	0.56
50	0.27	0.58	0.34	0.55
60	0.26	0.57	0.34	0.54
	E_S			
5	0.09	0.36	0.14	0.34
10	0.13	0.48	0.16	0.44
20	0.16	0.57	0.20	0.53
30	0.15	0.59	0.20	0.56
40	0.15	0.58	0.21	0.57
50	0.15	0.57	0.20	0.56
60	0.14	0.55	0.19	0.55

*P_{10} is 10th percentile; **P_{90} is 90th percentile;*

Table 1 shows that the efficiency factors display maxima after 20-40 years of injection. A hypothesis considered in this work suggests that during continuous active transport from the wellbore into the SRV, the efficiency factor terms increase. Later, when flow moves to unstimulated zones through natural fracture network, flow regime changes and efficiency factors start to decline. Thus, the presence of the maxima on efficiency factor curves indicates the change in flow regime from SRV dominated flow to flow in unstimulated zones. To test this hypothesis, RTA was used as described in the Methodology section.

Fig. 2a and Fig. 2b show total volume of injected CO_2 with their corresponding rates of injection for the four cases that define the maximum and minimum boundaries of the efficiency

factor, E_ϕ, listed in Table 1. In the description of the cases, the **R** (**R**eservoir pressure), **M** (**M**atrix permeability), **V** (Langmuir **V**olume), **D** (**D**ensity of natural fractures), **I** (**I**njection pressure), **P** (matrix **P**orosity), **T** (shale **T**hickness) symbols define input parameters given in Table S1 and are used in a combination with **L** or **H** designating the lower and upper boundary, respectively. Additional symbol, **S** (**S**hape), indicates SRV and is used with three numbers corresponding to three shapes of SRV [10]. The general shape of the injection rates and volumes is similar for the cases considered and we focus here on those defining limiting values of the efficiency factor, E_ϕ, for free phase storage in fractures and matrix pore space.

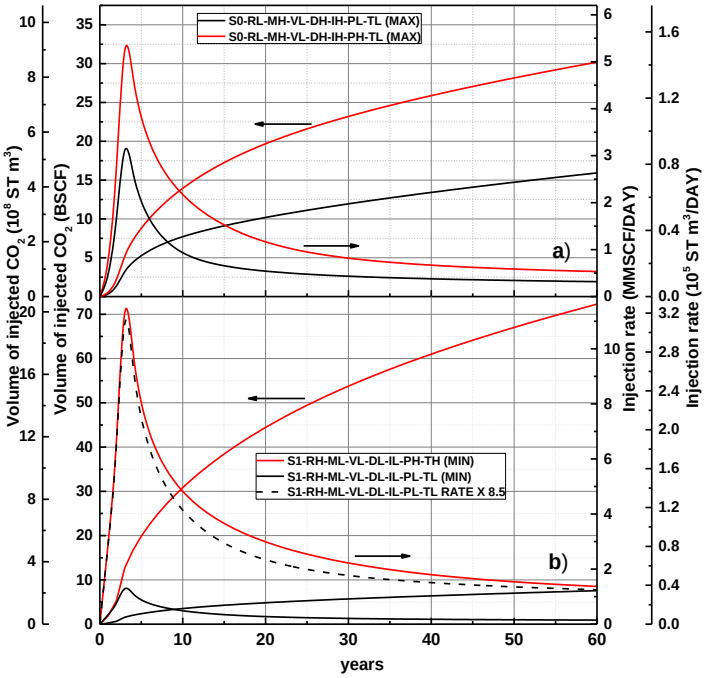

Fig. 2. Total volumes of carbon dioxide injected and injection rates as a function of time for **a)** the S0-RL-MH-VL-DH-IH-PH-TL and S0-RL-MH-VL-DH-IH-PL-TL cases and **b)** the S1-RH-ML-VL-DL-IL-PH-TH, S1-RH-ML-VL-DL-IL-PL-TL cases.

As shown in Fig. 2a and Fig. 2b, the injection rates experience peaks after 3 years of injection, beyond which the injection pressure is decreased monotonically until the end of injection period. The reason of the peak appearance after 3 years of injection is connected to a step-wise increase of the injection pressure during first three years. The injection wells used for geologic CO_2 sequestration into deep rock formations are designated as Class VI [37], which requires protecting underground sources of drinking water (USDWs). Hydraulic fractures provide direct preferential

pathways for upward fluid migration in shale-dominated strata located hundreds of feet above the hydraulically fractured layers [38]. The risk to USDW contamination could arise if the injection pressure is immediately set at the target values because of further hydraulic fracture propagation. To prevent that possibility in a field injection scenario, in this study the injection pressure is initially kept at 6.89 MPa during the first year, which is increased to 13.79 MPa for the second year, followed by the target pressure from the third year to the rest of the injection period (Table S1). Noticeably, cases with low porosity experience faster rate drop before leveling out after approximately 30-40 years (the dashed black line represents the 8.5 times increase in injection rate for the case with the low porosity value and is shown in Fig. 2b for convenience to compare against the high porosity case). The cases depicted in Fig. 2a and Fig. 2b indicate that low/high matrix permeability, low/high natural fracture density, low/high injection pressure, and high/low initial reservoir pressure are the main drivers of low/high reservoir efficiency. Besides, it appears that the regular SHAPE 0 / irregular SHAPE 1 (representing enlarged fractures at the heel and the toe of the lateral [10]) represents the most/less effective induced fracture distribution among three considered. This finding agrees with conclusion of another study [14], which showed that the analytical methods using only regular shaped SRVs [29,39] cannot accurately describe the well performance.

Fig. 3a and Fig. 3b show pressure distributions for the two cases that give minimum efficiency factors (Fig. 2b) at the end of the injection period. Because of the heterogeneous nature of the natural fracture network, the pressure distributions are non-uniform. Certain areas demonstrate a more pronounced flow reflecting better fracture connectivity (an analysis using several natural fracture realizations was performed for selected cases to ensure that every stochastic distribution provides statistically close results).

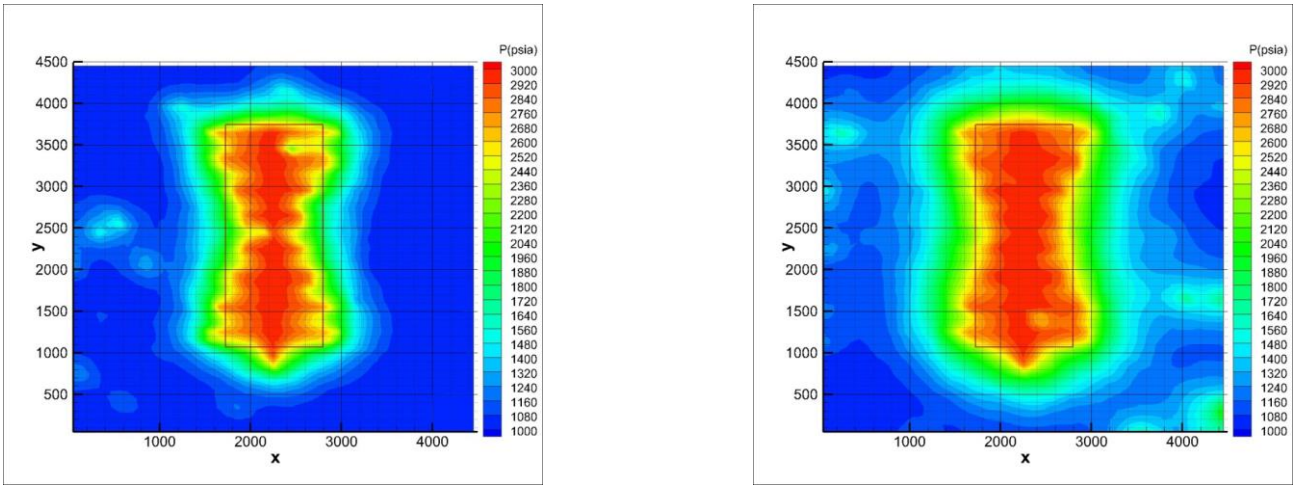

a) **b)**

Fig. 3. Pressure distributions in the middle horizontal plane of the shale reservoir after 60 years of injection for the **a)** S1-RH-ML-VL-DL-IL-PH-TH and **b)** S1-RH-ML-VL-DL-IL-PL-TL cases. The red rectangle designates the boundaries of the stimulated zone. The lateral is omitted for clarity.

The elevated pressure areas corresponding to CO_2 propagation are well within the reservoir boundaries for the case with high porosity (Fig. 3a), while the case with low porosity shows pressure propagation reaching the boundaries (Fig. 3b). This suggests that flow in the reservoir with low porosity experience a boundary effect resulting in a pseudo-steady flow regime with almost constant injection rates. Fig. 4a and Fig. 4b present the results of RTA for the four limiting cases depicted in Fig. 2a and Fig. 2b.

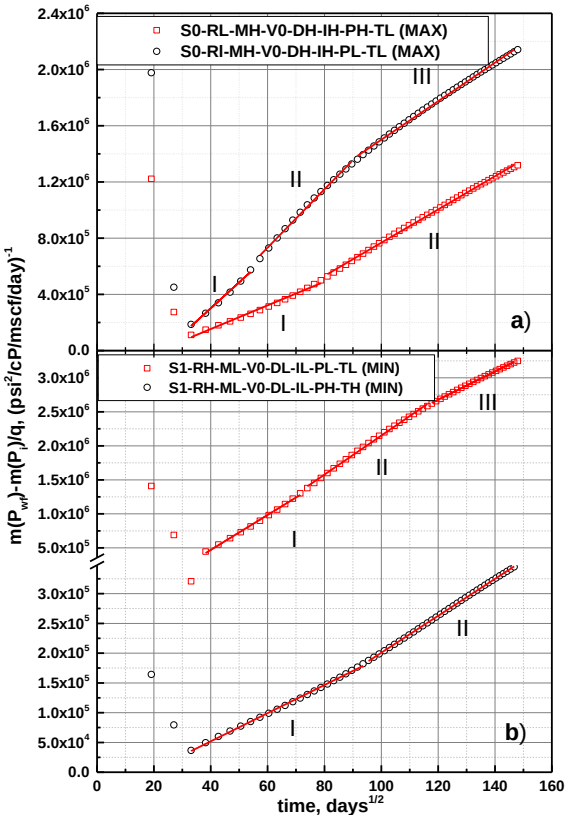

Fig. 4. The performance characteristic plot of pressure-normalized injection rates as a function of time at different flow regimes for **a)** the S0-RL-MH-V0-DH-IH-PH-TL and S0-RL-MH-V0-DH-IH-PL-TL cases and **b)** the S1-RH-ML-V0-DL-IL-PH-TH and S1-RH-ML-V0-DL-IL-PL-TL cases providing maximum and minimum efficiency factors, respectively.

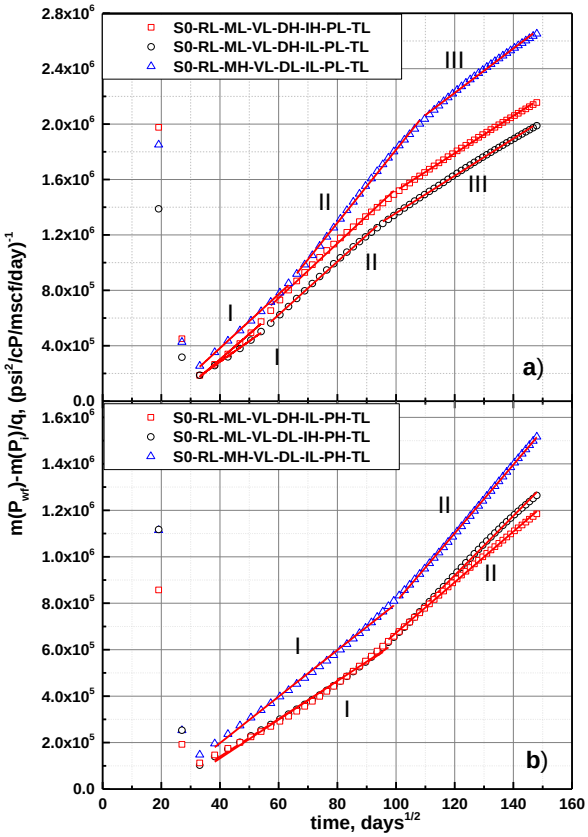

Fig. 5. The performance characteristic plot of pressure-normalized injection rates as a function of time at different flow regimes for **a)** the S0-RL-ML-VL-DH-IH-PL-TL, S0-RL-ML-VL-DH-IL-PL-TL, and S0-RL-MH-VL-DL-IL-PL-TL cases and **b)** for the S0-RL-ML-VL-DH-IL-PH-TL, S0-RL-ML-VL-DL-IH-PH-TL, and S0-RL-MH-VL-DL-IL-PH-TL cases demonstrating Regimes I-III and I-II, respectively.

The I, II, and III numbers on the plots identify Regimes I, II, and III, respectively. Indeed, the cases with low porosity values demonstrate three flow regimes, while high porosity of the shale reservoir leads to only two regimes. To further explore the effect of porosity on the flow regimes, RTA was performed for other cases. The results given in Fig. 5 have confirmed the above trend. The examples of pressure distributions are given in Fig. 6 showing that flow is localized with SRV for Regime I, continues within the reservoir boundaries through natural fractures and matrix pore for Regime II, and experiences the presence of reservoir's boundaries for Regime III. Obviously, the increase of the reservoir size would eliminate the prevailing Regime III at the end of injection period for cases with low porosity.

Table 2 collects bulk permeabilities, time periods, and efficiency factors for flow regimes in selected cases. This effective (bulk) formation permeabilities, *k*, are calculated using Equations

303 5-7 with contributions to the completion parameter estimated for each flow regime as described in
304 the last paragraph of Section III. The changes in flow regimes are associated with change in
305 reservoir permeability for CO_2 flow that includes "contributions" from induced and natural
306 fractures and matrix pores. The resulted permeabilities are computed to be on the orders of 10^{-2},
307 10^{-3}, and 10^{-5} md for Regimes I, II, and III, respectively (Table 2). Interestingly, the comparison
308 of the efficiency factors for the cases comprising only Regime II and cases comprising Regimes II
309 and III demonstrates that a transition from II to III does not lead to noticeable change in the value
310 of the efficiency factor.

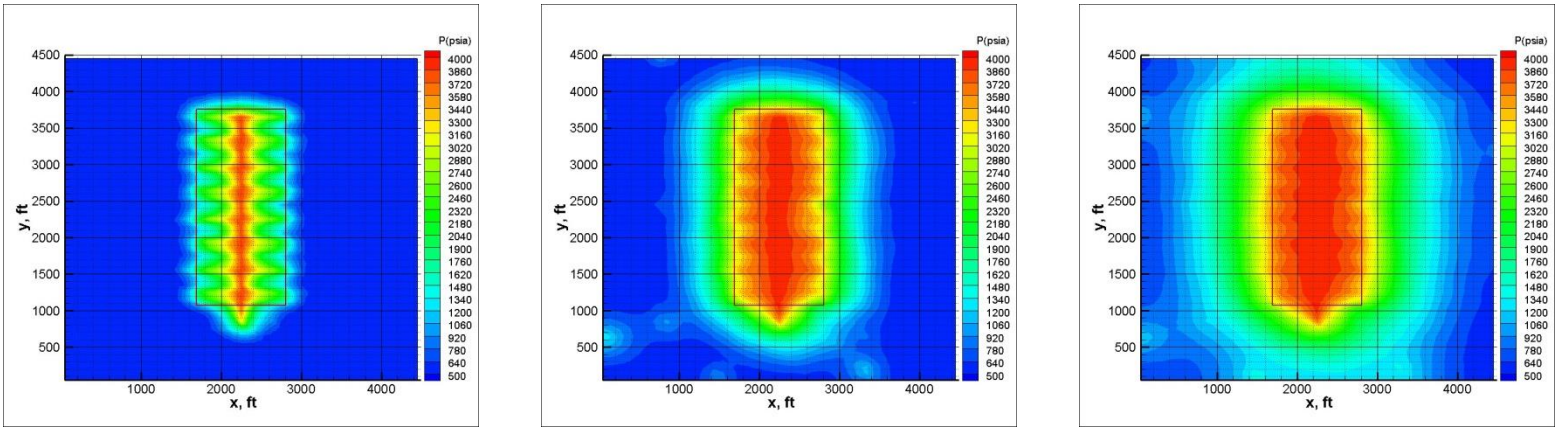

Fig. 6. Pressure distributions in the middle horizontal plane of the shale reservoir after **a)** Regime I; 10 years (case S0-RL-MH-VL-DH-IH-PH-TL); **b)** Regime II; 60 years (case S0-RL-MH-VL-DH-IH-PH-TL) and **c)** Regime III; 60 years (case S0-RL-MH-VL-DH-IH-PL-TL) of CO_2 injection. The red rectangle designates the boundaries of the stimulated zone. The lateral and hydraulic fracture locations are omitted for clarity.

311

Table 2

Bulk formation permeabilities (k_{bulk}) estimated using RTA for different flow regimes and corresponding efficiency factors for cases of interest.

case	Regime I			Regime II			Regime III		
	Range, years	k_{bulk}, md	Efficiency factors	Range, years	k_{bulk}, md	Efficiency factors	Range, years	k_{bulk}, md	Efficiency factors
S0-RL-MH-VL-DH-IH-PH-TL (MAX)	3-19	0.047	0.43-0.60	20-60	0.010	0.60-0.55	-	-	-
S0-RL-MH-VL-DH-IH-PL-TL (MAX)	3-9	0.026	0.56-0.59	10-23	0.009	0.59-0.56	24-60	1.826E-5	0.56-0.51
S1-RH-ML-VL-DL-IL-PH-TH (MIN)	3-30	0.012	0.17-0.29	31-60	0.004	0.29-0.27	-	-	-
S1-RH-ML-VL-DL-IL-PL-TL (MIN)	3-17	0.007	0.23-0.30	18-38	0.003	0.30-0.28	39-60	4.274E-6	0.28-0.26
S0-RL-ML-VL-DH-IL-PH-TL	3-25	0.019	0.33-0.47	26-60	0.008	0.48-0.45	-	-	-
S0-RL-ML-VL-DL-IH-PH-TL	3-25	0.037	0.33-0.54	26-60	0.009	0.55-0.54	-	-	-
S0-RL-MH-VL-DL-IL-PH-TL	3-27	0.032	0.26-0.44	28-60	0.006	0.46-0.44	-	-	-
S0-RL-ML-VL-DH-IL-PL-TL	3-9	0.014	0.41-0.47	10-28	0.005	0.47-0.45	29-60	1.011E-5	0.45-0.42
S0-RL-ML-VL-DH-IH-PL-TL	3-9	0.039	0.53-0.59	10-25	0.010	0.59-0.53	26-60	1.803E-5	0.53-0.51
S0-RL-MH-VL-DL-IL-PL-TL	3-12	0.023	0.37-0.46	13-33	0.006	0.46-0.46	34-60	1.339E-5	0.46-0.41

The behavior is in contrast with the transition from Regime I to II that leads to a clear change in the efficiency factors. In other words, continuous active transport of CO_2 as a free phase from the wellbore into SRV results in increasing the efficiency factors, which starts to decrease once CO_2 transitions occur into unstimulated zones through natural fracture network. The comparison of the permeability values and corresponding efficiency factors reveals that a high efficiency factor does not always translate to high bulk formation permeability and vice versa. In other words, the ability of a reservoir with high permeability to faster transmit fluids would not necessarily translate into a better storage potential of the fractured shale because their physical meaning signify potential ease of CO_2 injectivity and efficient utilization of storage volume, respectively.

Contribution of Adsorption to Storage

Among various parameters used to design simulation cases that account for variability in their magnitude per their values in the literature, adsorption of CO_2 is one of those parameters. Fig. 7a shows the amount of CO_2 stored for three limiting cases, which are storage without adsorption, storage with low adsorption, and storage with high adsorption (Table S1). The clay minerals and organic matter content in shale rock lead to high (e.g. large clay and organic content) or low (e.g. large inorganic content) adsorption, respectively. In the simulations performed in this work the difference in shale total organic content (TOC) and clay content is captured through low and high values of Langmuir constants (Table S1).The rocks favorable for adsorption can store ~44% more CO_2 than the rocks where there is no adsorption (% change from 23.2 to 33.4 bscf of stored CO_2 after 60 years of injection, Fig. 7b), or they can store 33% more CO_2 compared to rocks with relatively low adsorption (% change from 25.1 to 33.4 bscf, Fig. 7b). One can reasonably expect that mineralogy and organic matter of most shale reservoirs would facilitate adsorption that lies somewhere between those two limiting cases of low and high adsorption. Following that, the amount of CO_2 that can be stored on average by means of adsorption is ~26% of the CO_2 stored as free phase (the arithmetic average of % changes from 23.2 to 33.4 and 23.2 to 25.1 bscf, Fig. 7b).

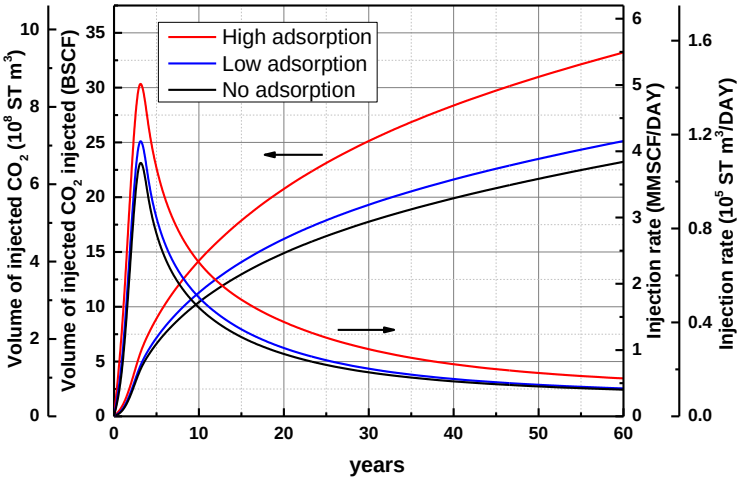

Fig. 7a. Total volumes of carbon dioxide injected and injection rates as a function of time for S0-RL-ML-VH-DH-IL-PH-TL (high adsorption), S0-RL-ML-VL-DH-IL-PH-TL (low adsorption), and S0-RL-ML-DH-IL-PH-TL (without adsorption) cases.

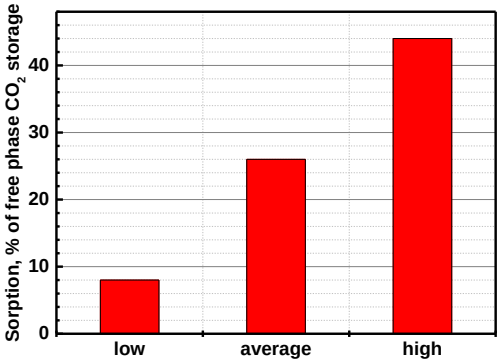

Fig. 7b. Adsorbed amounts of CO_2 relative to the amounts stored as a free phase (after 60 years of injection) based on the cases shown in Fig. 7a.

Several mechanisms of fluid transport exist in shale rocks at local scales that have been studied by researchers specifically to understand i) the uptake of fracturing fluid by shale [2,40-43], and ii) the non-Darcy flux of gas in organic matter or pores of the order of nanometers [44-47]. Although these local-scale mechanisms, which are often coupled together, have been studied by various researchers to some extent, there is lack of a simple mathematical model for these mechanisms in comparison to viscous flow and adsorption that were accounted by well-known Darcy's law and Langmuir isotherm, respectively, in this study. Therefore, these mechanisms are rarely accounted in numerical simulators, so it is difficult to assess their impact on flow regimes of CO_2 in shale reservoirs.

V. Conclusions

Numerical simulations of CO_2 injection into depleted fractured shale reservoirs were used to estimate volume of CO_2 stored for a range of reservoir parameters and injection scenarios, where the selected range is expected to cover parameter variability in gas-dominant organic-rich shale reservoirs at the national and regional scale. Numerical simulations were performed by considering free-phase and adsorbed phase as two mechanisms of CO_2 storage in shales. RTA was performed to identify flow regimes of CO_2 in depleted shale during the injection period. It was found that the

maximum efficiency factors occur within 15-30 years of injection for the studied cases and their maximum value is accompanied with a transition from the dominant transient flow regime within SRV (Regime I) to flow within unstimulated zones (Regime II). A practical implication of this result suggests that closely-spaced configuration of multiple horizontal wells would favor better storage efficiency because such a configuration would lead to better areal sweep of the reservoir, and hence efficient CO_2 storage. Unlike a closely-spaced configuration, multi-well configuration with large spacing would allow the CO_2 to move quickly through preferential pathways (e.g. a fractures), thus leading to inefficient reservoir sweep [1].

The bulk formation permeabilities estimated for different flow regimes using RTA show that high values of bulk permeability does not always translate to high efficiency factors; this is because, although, both high permeability and high efficiency factors are favorable for storage of CO_2 in depleted shale, their physical meaning signify potential ease of CO_2 injectivity and efficient utilization of storage volume, respectively.

Acknowledgment

This technical effort was performed in support of the National Energy Technology Laboratory's ongoing research under the RES contract DE-FE0004000. The simulations were carried out on NETL's High-Performance Computer for Energy and the Environment (HPCEE). This research was supported in part by an appointment to the National Energy Technology Laboratory Research Participation Program, sponsored by the U.S. Department of Energy and administered by the Oak Ridge Institute for Science and Education.

Disclaimer

This project was funded by the Department of Energy, National Energy Technology Laboratory, an agency of the United States Government, through a support contract with AECOM. Neither the United States Government nor any agency thereof, nor any of their employees, nor AECOM, nor any of their employees, makes any warranty, expressed or implied, or assumes any legal liability or responsibility for the accuracy, completeness, or usefulness of any information, apparatus, product, or process disclosed, or represents that its use would not infringe privately owned rights. Reference herein to any specific commercial product, process, or service by trade name, trademark, manufacturer, or otherwise, does not necessarily constitute or imply its

endorsement, recommendation, or favoring by the United States Government or any agency thereof. The views and opinions of authors expressed herein do not necessarily state or reflect those of the United States Government or any agency thereof.

References

[1] Singh H, Cai J. Screening improved recovery methods in tight-oil formations by injecting and producing through fractures. International Journal of Heat and Mass Transfer 2018;116,977–993.

[2] Zhou Z, Abass H, Li X, Teklu T. Experimental investigation of the effect of imbibition on shale permeability during hydraulic fracturing. Journal of Natural Gas Science and Engineering 2016;29,413-430.

[3] Busch A, Alles S, Gensterblum Y, Prinz D, Dewhurst DN, Raven MD, Stanjek H, Krooss BM. Carbon dioxide storage potential of shales. International Journal of Greenhouse Gas Control 2008; 2(3), 297-308.

[4] Edwards RW, Celia MA, Bandilla KW, Doster F, Kanno CM. A model to estimate carbon dioxide injectivity and storage capacity for geological sequestration in shale gas wells. Environmental science & technology 2015; 49(15), 9222-9229.

[5] Tao Z, Clarens A. Estimating the carbon sequestration capacity of shale formations using methane production rates. Environmental science & technology 2013; 47(19), 1318-11325.

[6] Schettler Jr PD, Parmely CR. Contributions to total storage capacity in Devonian shales. In SPE Eastern Regional Meeting. Society of Petroleum Engineers, 1991.

[7] Nuttal BC, Eble C, Bustin RM, Drahovzal, JA.Analysis of Devonian black shales in Kentucky for potential carbon dioxide sequestration and enhanced natural gas production. Greenhouse Gas Control Technologies 2005; 7, 2225-2228.

[8] Bacon DH, Yonkofski CM, Schaef HT, White MD, McGrail BP, CO_2 storage by sorption on organic matter and clay in gas shale. Journal of Unconventional Oil and Gas Resources 2015; 12, 123-133.

[9] Singh H, Cai J. A mechanistic model for multi-scale sorption dynamics in shale. Fuel 2018;234,996–1014 doi:10.1016/j.fuel.2018.07.104

[10] Myshakin EM, Singh H, Sanguinito S, Bromhal G, Goodman AL. Numerical estimations of storage efficiency for the prospective CO_2 storage resource of shales. International Journal of Greenhouse Gas Control 2018;76,24-31.

[11] Feng, Q, Xia T, Wang S, Singh H. Pressure Transient Behavior of Horizontal Well with Time-Dependent Fracture Conductivity in Tight Oil Reservoirs. Geofluids. 2017. https://doi.org/10.1155/2017/5279792.

[12] Singh H, Cai J. A Feature-Based Stochastic Permeability of Shale: Part 1—Validation and Two-Phase Permeability in a Utica Shale Sample. Transport in Porous Media 2018;1–34. doi:10.1007/s11242-018-1073-7

[13] Singh H, Cai J. A Feature-Based Stochastic Permeability of Shale: Part 2–Predicting Field-Scale Permeability. Transport in Porous Media 2018; 1–18. doi:10.1007/s11242-018-1076-4

[14] Suliman B, Meek R, Hull R, Bello H, Portis D, Richmond P. Variable stimulated reservoir volume (SRV) simulation: Eagle Ford shale case study, SPE-164546, In: SPE Unconventional Resource Conference, Woodlands, Texas, USA, 10-12 April, 2013.

[15] Ezulike DO, Adefidipe OA, Fu Y, Dehghanpour H, Virues CJ, Bearinger D. Flowback fracture closure: A key factor for estimating effective pore volume. SPE-175143-MS. In: SPE Annual Technical Conference and Exhibition, Houston, Texas, USA, 28-30 September, 2015.

[16] Beyadi H, Yuyi S, Junca-Laplace JP. Production analysis using Rate Transient Analysis. SPE-177293. In: SPE Eastern Regional Meeting, Morgantown, West Virginia, USA, 13-15 October, 2015.

[17] Bello RO. Rate transient analysis in shale gas reservoirs with transient linear behavior. Ph.D. thesis, Texas A&M University, 2009.

[18] Clarkson C. Production data analysis of unconventional gas wells: Review of theory and best practices. International Journal of Coal Geology 2013;109-110,101-146.

[19] Nobakht M, Clarkson CR. A New analytical method for analyzing linear flow in tight/shale gas reservoirs: constant-flowing-pressure boundary condition, SPE-143989, In: Americas Unconventional Gas Conference, Woodlands, Texas, USA, 12-16 June, 2012.

[20] Wattenbarger RA, El-Banbi AH, Villegas ME, Maggard JB. Production analysis of linear flow into fractured tight gas wells. SPE-39931, In: SPE Rocky Mountain Regional/Low-permeability reservoir symposium, Denver, USA, 5-8 April, 1998.

[21] Goodman A, Fukai I, Dilmore R, Frailey S, Bromhal G, Soeder D, Gorecki C, Peck W, Rodosta T, Guthrie G. Methodology for assessing CO_2 storage potential of organic-rich shale formations. Energy Procedia 2014;63,5178-5184.

[22] Senger K, Tveranger J, Braathen A, Olaussen S, Ogata K, Larsen L. CO_2 storage resource estimates in unconventional reservoirs: insights from a pilot-sized storage site in Svalbard, Arctic Norway. Environmental Earth Sciences 2015;73,3987-4009.

[23] Levine JS, Fukai I, Soeder DJ, Bromhal G, Dilmore RM, Guthrie GD, Rodosta T, Sanguinito S, Frailey S, Gorecki C, Peck W, Goodman AL. U.S. DOE NETL methodology for estimating the prospective CO_2 storage resource of shales at the national and regional scale. International Journal of Greenhouse Gas Control 2016;51,81–94.

[24] Frailey SM, Tucker O, Koperna GJ. The Genesis of the CO_2 Storage Resources Management System (SRMS). Energy Procedia, 2017, 114, 4262-4269.

[25] Bachu S. Review of CO_2 storage efficiency in deep saline aquifers. International Journal of Greenhouse Gas Control 2015; 40, 188-202.

[26] Gorecki CD, Ayash SC, Liu G, Braunberger JR, Dotzenrod NW. A comparison of volumetric and dynamic CO_2 storage resource and efficiency in deep saline formations. International Journal of Greenhouse Gas Control 2015; 42, 213-225.

[27] Industrial Carbon Management Initiative (ICMI), Shale Modeling Report. Kulga B, Ertekin T, Kalantari-Dahaghi A, Mohaghegh S, Siriwardane H, Myshakin E, Dilmore R, Wyatt C, Siegel J. NETL Technical Report Series, U.S. Department of Energy, National Energy Technology Laboratory: Morgantown, West Virginia, USA, 2013.

[28] FRACGEN/NFFLOW. Discrete Fracture Reservoir Simulator, Version 14.9, 2014. https://edx.netl.doe.gov/dataset/fracgen-and-nfflow-version-14-9 (accessed on February 13, 2019).

[29] Agarwal RG, Gardner DC, Kleinsteiber SW, Fussel DD. Analyzing well production data using combined type-curve and decline-curve analysis concepts. SPE-57916-PA. SPE Reservoir Eveluation and Engineering 1999;2,478-486.

[30] Anderson DM, Mattar L. An improved pseudo-time for gas reservoirs and significant transient flow, Paper CIPC 2005-114. In: Canadian International Petroleum Conference, Calgary, Canada, 7-9 June, 2005.

[31] Ibrahim M, Wattenberger RA. Rate dependence of transient linear flow in tight gas wells, Paper CIPC 2005-057, In: Canadian International Petroleum Conference, Calgary, Canada, 7-9 June, 2005.

[32] Ibrahim M, Wattenberger RA. Analysis of rate dependence in transient linear flow in tight gas wells. SPE 100836, In: Abu Dhabi International Petroleum Exhibition and Conference, Abu Dhabi, UAE, 5-8 November, 2006.

[33] Burke L. Carbon dioxide fluid-flow modeling and injectivity calculations: U.S. Geological Survey Scientific Investigations Report 2011–5083, 16 p, 2011.

[34] Bahrami N, Pena D, Lusted I. Well test, rate transient analysis and reservoir simulaiton for characterizing mutli-fractured unconventional oil and gas reservoirs. Journal of Petroleum Exploration and Production Technology 2016;6,675-689.

[35] Bachu S, Bonijoy D, Bradshaw J, Burruss R, Holloway S, Christensen NP, Mathiassen OM. CO_2 storage capacity estimation: methodology and gaps. International Journal of Greenhouse Gas Control 2007;1, 430–443.

[36] Gorecki CD, Holubnyak YI, Ayash SC, Bremer JM, Sorensen JA, Steadman EN, Harju JA. A new classification system for evaluating CO_2 storage resource/capacity estimates. SPE 126421-MS-P, In: Society of Petroleum Engineers International Conference on CO_2 Capture, Storage, and Utilization, San Diego, California, USA, 2-4 November, 2009.

[37] United States Environmental Protection Agency (US EPA). Final Class VI Guidance Documents. EPA 816-R-18-001: 212, 2018.

[38] Myshakin EM, Siriwardane H, Lindner E, Sams N, King S, McKoy M. Numerical simulations of vertical growth of hydraulic fractures and brine migration in geological formations above the Marcellus shale, Journal of Natural Gas Science and Engineering 2015;27,531-544.

[39] Bello RO, Wattenberger RA. Rate Transient Analysis in naturally fractured shale gas reservoirs. SPE-114591. In: CIPC/SPE Gas Technology Symposium, Calgary, Canada, 16-19 June, 2008.

[40] Singh H. A critical review of water uptake by shales. Journal of Natural Gas Science and Engineering 2016;34,751-766.

[41] Makhanov K, Habibi A, Dehghanpour H, Kuru E, Liquid uptake of gas shales: a workflow to estimate water loss during shut-in periods after fracturing operations. Journal of Unconventional Oil Gas Resources 2014;7,22-32.

[42] Roshan H, Ehsani S, Marjo CE, Andersen MS, Acworth RI. Mechanisms of water adsorption into partially saturated fractured shales: an experimental study. Fuel 2015;159,628-637.

[43] Meng M, Ge H, Ji W, Shen Y, Su S. Monitor the process of shale spontaneous imbibition in co-current and counter-current displacing gas by using low field nuclear magnetic resonance method. Part 1. Journal of Natural Gas Science and Engineering 2015;27,336-345.

[44] Singh H, Javadpour F. A new non-empirical approach to model transport of fluids in shale gas reservoirs. In: Unconventional Resources Technology Conference, Denver, Colorado, USA, 12-14 August, 2013.

[45] Singh H, Javadpour F. Langmuir slip-Langmuir sorption permeability model of shale. Fuel 2016;164,28–37.

[46] Singh H, Javadpour F, Ettehadtavakkol A, Darabi H Non-empirical apparent permeability of shale. SPE Reservoir Evaluation & Engineering 2014;17,414–24.

[47] Kang SM, Fathi E, Ambrose RJ, Akkutlu IY, Sigal RF. Carbon dioxide storage capacity of organic-rich shales. SPE 134583, SPE Journal 2011;16,842–855.